Description of proton-neutron mixed-symmetry states near ^{132}Sn within a realistic large scale shell model

K. Sieja,[1,2] G. Martínez-Pinedo,[1] L. Coquard,[2] and N. Pietralla[2]
[1]*GSI-Helmholtzzentrum für Schwerionenforschung mbH, Planckstrasse 1, D-64220 Darmstadt, Germany*
[2]*Institut für Kernphysik, Technische Universität Darmstadt, D-64289 Darmstadt, Germany*
(Received 4 October 2009; published 18 November 2009)

Large scale shell-model calculations with an effective interaction derived from the realistic G-matrices were performed for $N = 80$ isotones for which so-called mixed-symmetry states were recently observed experimentally. Calculated spectra are shown to be in good agreement with data. The calculated transition rates reveal the necessity of modifying the strength of the pairing interaction. The structure of mixed-symmetry 2^+ states is analyzed in terms of seniority components and by decomposition into the Q-phonon scheme.

DOI: 10.1103/PhysRevC.80.054311 PACS number(s): 21.60.Cs, 21.10.−k, 27.60.+j

I. INTRODUCTION

The nuclear many-body system exhibits three generic features that make it an intriguing object of scientific studies. These are (i) collectivity originating in its strongly correlated many-body nature, (ii) shell structure originating in the fermionic nature of its constituents, and (iii) the isospin degree of freedom originating in the approximate charge independence of the strong interaction between its two types of constituents, protons and neutrons. Most intriguing are nuclear structure phenomena in which these features are equally important and compete with each other. One class of such phenomena is represented by collective isovector valence-shell excitations such as proton-neutron mixed-symmetry states [1–3].

Mixed-symmetry states (MSSs) have first explicitly been formulated [4–6] as valence-shell excitations in the algebraic interacting boson model (IBM) [7]. The existence of mixed-symmetry states has been established over the last 25 years in axially deformed nuclei (e.g., [1,2], and references therein), in deformed nuclei with softly fluctuating triaxiallity [8–10], and in vibrational nuclei (e.g., [11,12]). Owing to an increasing amount of data on MSSs of vibrational nuclei [3], the focus of the scientific discussion has recently shifted to the observation that the lowest-lying mixed-symmetry modes in some vibrational nuclei are concentrated in single quantum states [12–16], whereas they are fragmented into several states in others [8,17–19]. In the $N = 80$ isotone ^{138}Ce, the observed fragmentation has been interpreted [18] in terms of the lack of shell stabilization because of the underlying proton shell structure. This conjecture has been supported by microscopic calculations using the empirical quasiparticle phonon model [19,20]. An alternative approach that is more directly founded on the fundamental nuclear interaction might be offered by realistic shell-model (SM) calculations.

Empirical [20,21] SM calculations for MSSs have already been done in the mass regions $A = 90$ and $A = 140$. There has also been an attempt at realistic calculations for $N = 52$ isotones in the $A = 90$ mass region [22]; however, information on its capability of consistently describing the entire low-energy nuclear level scheme is missing. Therefore it is desirable to advance to a comprehensive realistic SM calculation for MSSs that consistently describes other low-energy features of the nuclear structure under study. The $N = 80$ isotones near ^{132}Sn are very attractive objects for such an endeavor because recent data on this isotonic chain contain both nuclei with a strongly pronounced isolated MSS [15,20] and nuclei with a fragmented MSS [17].

In this article, we perform a fully microscopic study of the MSSs in some $N = 80$ isotones within the SM framework, using an effective Hamiltonian based on the realistic nucleon-nucleon interaction. We start the discussion with a review of the SM calculations and effective interaction, which we use in Sec. II. Then, we show the spectra and transition rates for nuclei of interest in Sec. III. The discussion of the MSSs is divided into several parts. First, we study the structure of calculated 2^+ states and fragmentation of the $M1$ transition strengths as obtained with the realistic interaction in Sec. IV. To obtain further insight into the calculated transition rates, we project the calculated wave functions onto Q-phonon symmetric and mixed-symmetric states in Sec. IV A. Next, we analyze the influence of the pairing interaction on the observed fragmentation of $B(M1)$ values. Furthermore, we examine the evolution of magnetic moments of the first excited and MS 2^+ states and possible microscopic conditions that lay the basis for the formation of MSSs in this region. Finally, a summary is given in Sec. V.

II. SHELL-MODEL FRAMEWORK

The derivation of an accurate effective interaction has always been the main difficulty of the nuclear shell model theory. Although much progress has been obtained in this domain, it is still not possible to obtain interactions that simultaneously prove to be consistent with the nucleon-nucleon phase shifts and provide a good spectroscopy in a wide mass region. It has been shown, however, that phenomenological corrections applied to the monopole part of the realistic Hamiltonians can greatly improve the accuracy of the shell-model description of the many-body data [23,24]. Such a procedure has been recently followed [25] within the *gdsh*-shell, with the $0g_{7/2}$, $1d_{5/2}$, $1d_{3/2}$, $2s_{1/2}$, and $h_{11/2}$ orbitals for both protons and neutrons. As a starting point

for the empirical fit, the microscopically derived G-matrix interaction with the Bonn-C potential was used. Then, the low-lying states of all even-even and even-odd semimagic nuclei within the 50–82 valence space, all even-odd Sb isotopes and $N = 81$ isotones, and some known odd-odd nuclei around ^{132}Sn were included in the fit. Such a phenomenologically corrected interaction, dubbed hereinafter GCN5082, allowed for the reproduction of the experimental excitation energies of 320 states in 87 nuclei with a rms error of 110 keV [25]. The greatest deviations from the original G-matrix concerned the monopoles. However, modifications of certain pairing and other multipole matrix elements were also applied to further increase the match with data.

The GCN5082 interaction has already been explored in calculations of $\beta\beta$ decays of ^{124}Sn, ^{128}Te, ^{130}Te, ^{136}Te, and ^{136}Xe [26–28]. Recently, it has also been used in the investigations of the excitation spectra of ^{134}Xe up to 5 MeV, and an excellent agreement between theory and experiment was obtained for the levels of both parities [29]. In this article, we apply the GCN5082 interaction to study the $N = 80$ isotones, from Te to Nd, with special attention paid to the electromagnetic transition rates and the structure of the excited 2^+ states, among which the mixed-symmetric ones are observed in this region. The calculations are carried out using the SM codes NATHAN and ANTOINE [24,30]. A full diagonalization within the *gdsh* valence space is performed for ^{132}Te, ^{134}Xe, ^{136}Ba, and ^{138}Ce, whereas for ^{140}Nd, truncated calculations are carried out up to seniority 10, which ensures converged results for the computed quantities.

III. PROPERTIES OF $N = 80$ ISOTONES

Let us start the discussion with presenting the calculated properties of the $N = 80$ isotones, that is, excitation energies and electromagnetic transition rates between the low-lying states, obtained with the effective interaction described previously. In this work, we are interested mostly in the lowest four excited 2^+ levels, which are located below 2.5 MeV in all studied nuclei. Therefore we expect that the major physical features can be fairly reproduced within the *gdsh* valence space. As seen from Figs. 1–5, a satisfactory agreement is found for the excitation spectra of all nuclei, including the energies of several excited 2^+ levels. However, in the calculations of the $E2$ transition strengths, the values of proton and neutron effective charges had to be enhanced to account for the missing cross-shell excitations. We have adjusted $e^n_{\rm eff} = 0.7$ and $e^p_{\rm eff} = 1.7$ to reproduce well $2^+_1 \to 0^+_1$ transitions, and we have adopted those values to calculate the remaining $B(E2)$ values. The results are summarized in Table I. Shown are only transitions for which experimental values are known.

Owing to the lack of the spin-orbit partners of the biggest orbits within the *gdsh* space, that is, the $g_{9/2}$ and $h_{9/2}$, also, a renormalization of the g factors is necessary to reproduce the experimental magnetic moments. In Ref. [31], the measured g factors for Xe isotopes have been reported, and SM calculations were performed in the *gdsh* valence space using a surface-δ interaction. The single-particle g factors

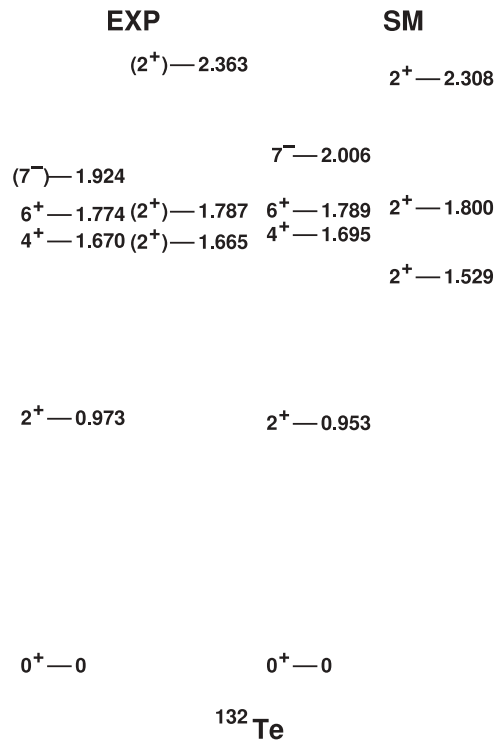

FIG. 1. SM and experimental (EXP) low-lying spectra of ^{132}Te.

were tuned in the calculations to reproduce the data. In this article, we adopt those effective g values, that is, $g^\pi_l = 1.13$, $g^\nu_l = 0.02$, $g^\pi_s = 4.04$, and $g^\nu_s = -2.65$, that, in particular, allow us to reproduce accurately the magnetic moment of the first excited 2^+ state in ^{134}Xe: We calculate the magnetic

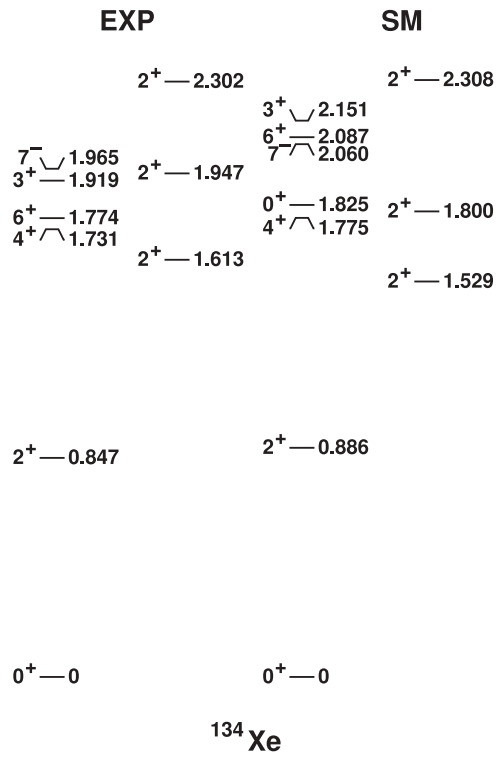

FIG. 2. SM and EXP low-lying spectra of ^{134}Xe.

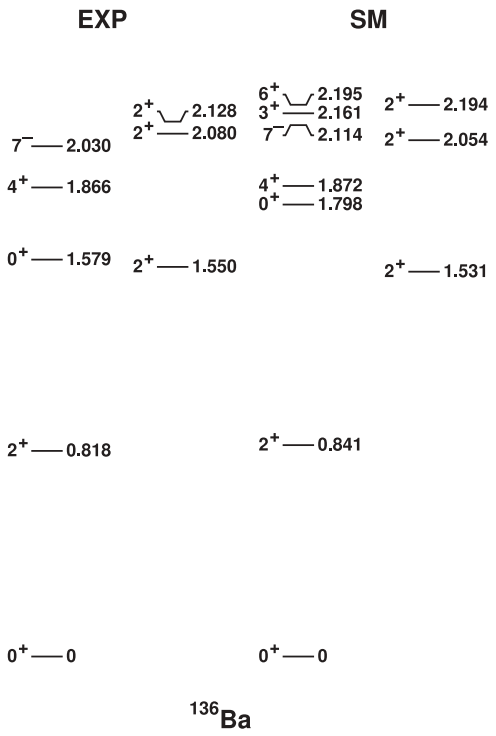

FIG. 3. SM and EXP low-lying spectra of ^{136}Ba.

moment of 0.683 μ_N to be compared with the measured value of 0.708(14) μ_N.

The calculated $M1$ transition rates are shown in Fig. 6(a) for ^{134}Xe, ^{136}Ba, and ^{138}Ce in comparison to available experimental data. As can be seen, the fragmentation and

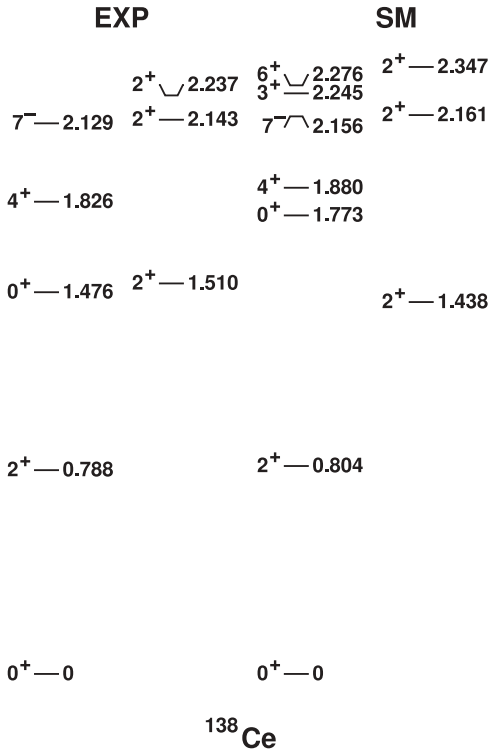

FIG. 4. SM and EXP low-lying spectra of ^{138}Ce.

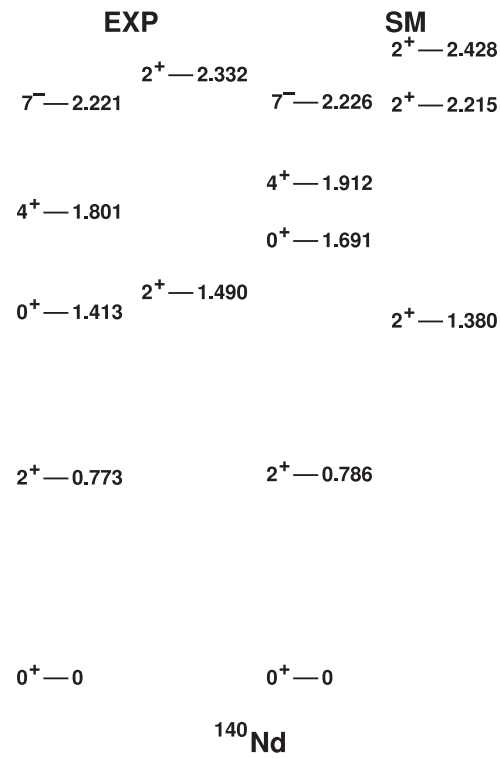

FIG. 5. SM and EXP low-lying spectra of ^{140}Nd.

magnitudes of $M1$ transitions are not reproduced accurately. Notably, we predict a considerable transition from the 2^+_2 situated in all nuclei around 1.5 MeV to the 2^+_1, which is not seen in experiment. The calculated $M1$ strength distributions remain indifferent to small changes of spin-orbital g factors.

The deviations from experimental values in both types of transition rates concerning the 2^+ states suggest that the microscopic wave functions calculated with the GCN5082 interaction may not posses the proper structure. In the following paragraphs, we study those wave functions in detail and compare their structure to that suggested by the IBM-2 model.

IV. MIXED-SYMMETRY STATES

In the proton-neutron IBM-2 [7], the multiphonon states are classified according to the quantum number called F spin, which extends the concept of isospin to proton and neutron bosons. The states with maximum F spin are then fully symmetric to the exchange of proton and neutron bosons. States with nonmaximum F spin are said to have proton-neutron mixed symmetry. In this article, we concentrate on MSSs with F-spin quantum number $F = F_{\max} - 1$ only. The IBM-2 model defines a specific signature for states of a given symmetry: Strong $E2$ transitions connect the states with the same F spin differing by one d-boson, whereas states having the same number of bosons but differing in F spin by one unit are connected by strong $M1$ transitions [7,32].

According to the IBM-2 model, the lowest MSS in vibrational nuclei is a one-quadrupole phonon 2^+ state characterized by a large $M1$ transition rate to the first excited 2^+ state. In

TABLE I. Theoretical $B(E2;\ J_f \to J_i)$ values (in e^2 fm^4) in comparison to available data.

	J_i	J_f	SM	EXP	Ref.
^{132}Te	2_1^+	0_1^+	323	344(34)	[38]
	6_1^+	4_1^+	142	132(8)	[39]
^{134}Xe	2_1^+	0_1^+	561	623(45)	[40]
	2_2^+	2_1^+	537	815(81)	[15]
	2_2^+	0_1^+	140	30.1(20)	[15]
	2_3^+	2_1^+	181	22.8(16)	[15]
	2_3^+	0_1^+	15	29.3(28)	[15]
	2_4^+	2_1^+	60	5.70 (41) or 228(16)[a]	[15]
	2_4^+	0_1^+	10	25.7(24)	[15]
	4_1^+	2_1^+	480	472(33)	[40]
^{136}Ba	2_1^+	0_1^+	773	798(6)	[41]
	0_2^+	2_1^+	35	<2908	[42]
	2_2^+	2_1^+	1084	623(166)	[41]
	2_2^+	0_1^+	180	32.4(79)	[41]
	2_3^+	2_1^+	60	83(166)	[42]
	2_3^+	0_1^+	33	5.4(29)	[42]
	2_4^+	2_1^+	14.5	0.012(12)	[42]
	2_4^+	0_1^+	14	90(10)	[36]
	4_1^+	2_1^+	700	582(249)	[42]
	6_1^+	4_1^+	1.2	38.6(9)	[43]
^{138}Ce	2_1^+	0_1^+	974	898(59)	[44]
	2_2^+	2_1^+	1507	1186(85)	[17]
	2_2^+	0_1^+	187	49.1(34)	[17]
	2_3^+	2_1^+	21	318(38)	[17]
	2_3^+	0_1^+	29	24.1(17)	[17]
	2_4^+	2_1^+	3	27.5(42)	[17]
	2_4^+	0_1^+	5	78.8(68)	[17]

[a]Two different values for the two different values of δ in Ref. [15].

our SM calculations, it appears to be dominantly present in the third excited states of ^{134}Xe, ^{136}Ba, and ^{138}Ce.

Figure 7 shows the calculated and experimental energies of these two states. Looking qualitatively to the evolution of the MSSs when protons are added, a good agreement with experiment is found. One observes that the $2^+_{\rm MS}$ state is shifted to higher energy with increasing proton number, whereas the 2_1^+ energy is at the same time lowered [15,22]. The increase of the energy of the MS state is in agreement with the systematics of the 2_1^+ states in $N = 82$ isotones; thus one may suppose that MS states are due mostly to a proton excitation. In addition to the experimentally known cases, we have added as well the calculated values for the neighboring ^{132}Te and ^{140}Nd. In the case of the latter, only a truncated calculation was performed at the $\nu = 10$ level. Our SM calculations predict that for ^{132}Te, the second excited 2^+ state calculated at energy 1.44 MeV possesses the MS, whereas for ^{140}Nd, it is the third calculated 2^+ state at an energy of about 2.3 MeV. As can be seen, the predictions for these two nuclei follow the systematics very well.

However, as formerly mentioned, the $M1$ transition rates between different 2^+ states calculated in SM do not agree fully with experimental values. To understand better those deviations, we have studied the structure of the SM wave functions. In Table II, we have listed the dominant components in terms of proton-neutron couplings for 2^+ states of interest.

TABLE II. Contributions of different seniority components (in percentage) to the SM wave functions calculated with the GCN5082 interaction. In the case of $\nu = 2$, we show in parentheses proton-neutron (π, ν) contributions.

	J^π	$\nu = 0$	$\nu = 2$ (π, ν)	$\nu = 4$	$\nu = 6$	$\nu > 6$
^{132}Te	0^+	89	0	11	0	0
	2_1^+	0	92 (39,53)	8	0	0
	2_2^+	0	81 (46,35)	19	0	0
^{134}Xe	0^+	78	0	20	2	0
	2_1^+	0	83 (31,52)	20	7	0
	2_3^+	0	60 (17,43)	31	9	0
^{136}Ba	0^+	72	0	25	2	1
	2_1^+	0	77 (27,51)	12	10	1
	2_3^+	0	56 (18,38)	24	18	2
^{138}Ce	0^+	66	0	29	3	1
	2_1^+	0	72 (24,48)	14	12	2
	2_3^+	0	54 (18,37)	25	17	4
^{140}Nd	0^+	62	0	32	4	2
	2_1^+	0	68 (21,47)	16	14	2
	2_3^+	0	48 (16,32)	24	22	6

In Table III, we have shown the percentage of different seniority components contained in the wave functions of the ground state, the first excited 2^+ states, and the MS state. For seniority $\nu = 2$, we have distinguished the proton and neutron percentage contributions in parentheses. Finally, in Table IV, we have shown the occupation numbers of individual proton and neutron shells for those states.

First of all, the calculated states appear to be quite complex, and no configuration is clearly favored. Looking to the couplings of proton and neutron subspaces, one can see that the realistic wave functions go beyond the assumptions of the IBM-2 model, in which the states can be described with only s and d bosons. While the first 2^+ state is mostly because of a $2^+ \otimes 0^+$ type of coupling, the MS states contain only $\sim$60% of such a structure, and the contribution of the $2^+_\nu \otimes 2^+_\pi$ and higher spin couplings becomes increasingly important with increasing proton number. One can also notice that the

TABLE III. Structure of calculated first excited and MS 2^+ states. Only several dominant components are listed. The results concern SM calculations with the original GCN5082 interaction.

	J^π	$2^+_\nu \otimes 0^+_\pi$	$0^+_\nu \otimes 2^+_\pi$	$2^+_\nu \otimes 2^+_\pi$
^{132}Te	2_1^+	53	40	4
	2_2^+	45	46	2
^{134}Xe	2_1^+	54	32	6
	2_3^+	44	21	13
^{136}Ba	2_1^+	54	28	6
	2_3^+	40	23	10
^{138}Ce	2_1^+	51	26	6
	2_3^+	38	23	11
^{140}Nd	2_1^+	51	24	6
	2_3^+	35	21	13

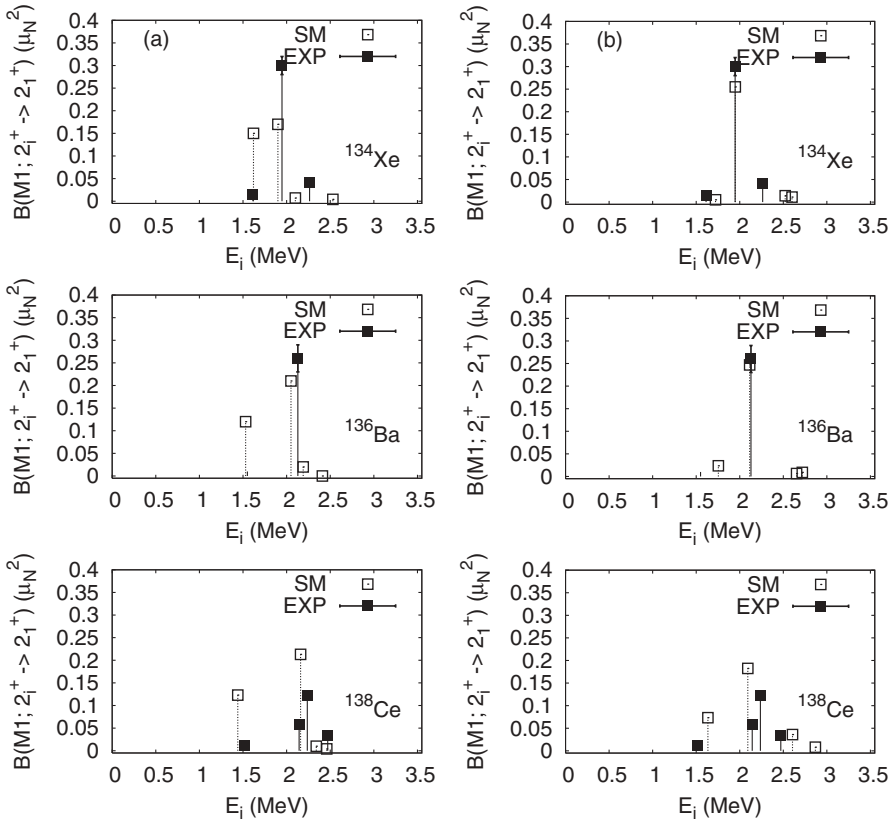

FIG. 6. Theoretical (open squares) and experimental (solid squares) $M1$ transition rates from excited 2_i^+ states to the 2_1^+ state: (a) calculations with the GCN5082 interaction; (b) calculations with the same interaction but with modified pairing matrix elements (see text for further details).

first excited 2^+ state is neutron in character, as expected; surprisingly, the MS state has a similar, though less clean, nature. This complexity is further reflected in the mixing of different seniority components, as seen from Table II. The ground state is formed at around 70% by the seniority $\nu = 0$ component. The first excited 2^+ state is predominantly a seniority 2 state (∼80%), but the supposed mixed-symmetry one-phonon state (the third excited 2^+ state in the shown cases) contains only 55%–60% of the $\nu = 2$ component. On the basis of the IBM-2 model, one would expect that the 2_1^+ and $2_{\rm MS}^+$ states originate from the linear combinations of proton and neutron one-phonon (i.e., $\nu = 2$) components with opposite signs and inverted amplitudes (see, as well, Sec. IV A). Taking the ^{134}Xe as the instance, both the 2_1^+ and $2_{\rm MS}^+$ states are formed by the $\nu = 2$ neutron component with a quite similar probability (54% and 44%, respectively) and by a proton component with 32% and 21% probability, respectively. We have verified that the signs of the amplitudes of dominant

TABLE IV. Occupations of proton and neutron valence shells in the states of interest. The results concern SM calculations with the original GCN5082 interaction.

	J^π	$\pi d_{5/2}$	$g_{7/2}$	$s_{1/2}$	$d_{3/2}$	$h_{11/2}$	$\nu d_{5/2}$	$g_{7/2}$	$s_{1/2}$	$d_{3/2}$	$h_{11/2}$
^{132}Te	0^+	0.32	1.41	0.02	0.08	0.17	5.85	7.85	1.82	3.45	11.03
	2_1^+	0.20	1.58	0.03	0.09	0.10	5.86	7.88	1.66	3.33	11.27
	2_2^+	0.20	1.62	0.02	0.07	0.09	5.86	7.86	1.75	3.42	11.10
^{134}Xe	0^+	0.85	2.57	0.04	0.16	0.38	5.83	7.84	1.78	3.37	11.18
	2_1^+	0.78	2.66	0.06	0.17	0.32	5.84	7.85	1.61	3.24	11.46
	2_3^+	0.99	2.47	0.06	0.18	0.30	5.92	7.93	1.88	3.65	10.61
^{136}Ba	0^+	1.53	3.48	0.08	0.25	0.66	5.82	7.82	1.75	3.33	11.28
	2_1^+	1.51	3.52	0.10	0.26	0.61	5.82	7.84	1.59	3.21	11.54
	2_3^+	1.76	3.35	0.12	0.26	0.51	5.90	7.92	1.85	3.58	10.75
^{138}Ce	0^+	2.21	4.31	0.13	0.35	1.0	5.81	7.81	1.73	3.30	11.35
	2_1^+	2.18	4.34	0.16	0.36	0.95	5.80	7.82	1.59	3.20	11.59
	2_3^+	2.39	4.23	0.18	0.38	0.82	5.90	7.92	1.86	3.47	10.84
^{140}Nd	0^+	2.88	5.03	0.19	0.47	1.43	5.80	7.80	1.70	3.28	11.42
	2_1^+	3.02	5.02	0.25	0.53	1.18	5.92	7.91	1.78	3.54	10.85
	2_3^+	3.01	5.04	0.32	0.53	1.09	5.82	7.82	1.65	3.29	11.42

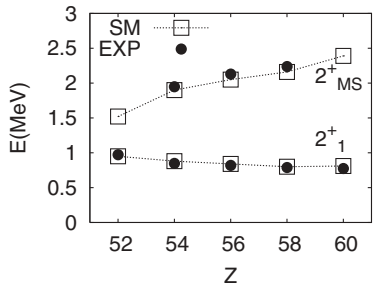

FIG. 7. Evolution of calculated and theoretical energies of the first excited 2^+ state (2^+_1) and the mixed-symmetry state (2^+_{MS}) in $N = 80$ isotones.

components in 2^+_1 and 2^+_{MS} are indeed opposite. A very similar situation is found in other nuclei.

To make this analysis more transparent, in the next section, we perform expansion of the SM wave functions into the symmetric and mixed-symmetric combinations of proton and neutron one-quadrupole phonon states.

A. *Q*-phonon scheme

In the Q-phonon scheme, as proposed by Otsuka [33], the unnormalized wave functions of the lowest-lying fully symmetric and mixed-symmetry states can be represented as quadrupole excitations over the strongly correlated ground state $|0^+_1\rangle$:

$$|2^+_1\rangle = Q_S|0^+_1\rangle, \qquad |2^+_{MS}\rangle = Q_{MS}|0^+_1\rangle, \tag{1}$$

where $Q_S = Q_p + Q_n$ and $Q_{MS} = Q_p - \alpha Q_n$ are the symmetric and mixed-symmetric quadrupole operators and the α coefficient is obtained from orthonogalization (normalization coefficients are skipped for simplicity). In such a scheme, it is particularly apparent that the 2^+_{MS} state is a one-phonon excitation that has a proton and neutron $E2$ excitation matrix element of about the same size as the first excited 2^+_1 state; however, because of the different signs of proton and neutron contributions, the total $E2$ excitations to these states should be different. More clearly, the $M1$ value connecting them should be particularly strong because of the isovector character of the transition operator.

The Q-phonon scheme may be a useful tool to interpret the MS structure of fully microscopic wave functions like those obtained in our SM calculations. To understand the magnitudes and fragmentation of calculated $M1$ transition rates, we have constructed the symmetric (S) and mixed-symmetric (MS) states, as defined in Eq. (1), by the linear superposition of the proton and neutron quadrupole excitations built on the calculated $|0^+\rangle$ ground state. Those states were further orthonormalized and projected onto SM 2^+ states by means of the Lanczos structure function method with 50 iterations. However, two issues need to be mentioned here. First, the SM wave function of the ground state may not correspond to an F-spin symmetric ground state of the IBM-2 model. Second, because we work in a constrained model space, effective quadrupole operators should be used in SM calculations. To build the symmetric and mixed-symmetric states from Eq. (1), we have, however, applied the same effective charges for neutrons and protons, equal to 1.

The result of such a procedure is shown in Fig. 8(a). One can see that the first excited 2^+ state is built up mostly by the

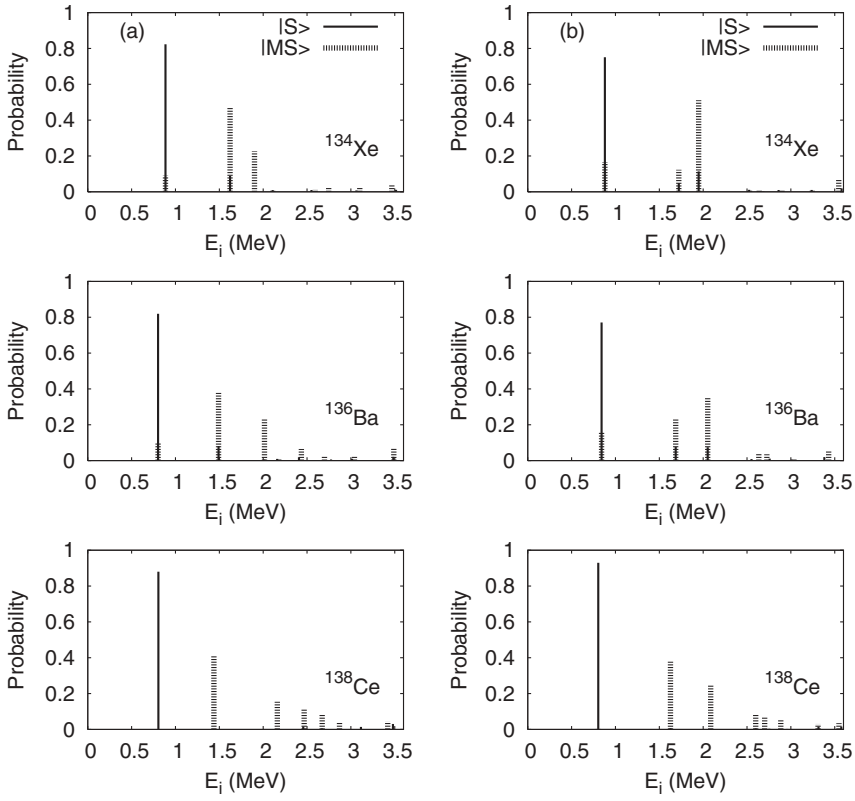

FIG. 8. Symmetric (S, solid line) and mixed-symmetric (MS, dashed line) Q-phonon states projected onto SM 2^+ states calculated with (a) the GCN5082 interaction and with (b) the GCN5082 interaction with modified pairing matrix elements (see text for more details).

symmetric component. On the contrary, the MSS is fragmented into several states; an especially pronounced strength is going to the second excited 2^+ state situated around 1.5 MeV, which explains the significant $B(M1)$ value that we calculate from this state to the first 2^+ state. In ^{138}Ce, one observes that the mixed-symmetric component is shifted to a higher energy and no longer contributes to the first 2^+ state.

As has been discussed, the calculated states have a quite complicated seniority structure in comparison to the simple assumptions of the Q-phonon scheme. To make the calculated states more pure in seniority, we have generated matrix elements of the isovector and isoscalar pairing Hamiltonians, as defined, for example, in Ref. [34], with a coupling constant $G = 0.1$ and added them to the realistic interaction. For instance, the $V^{T=1,J=0}_{h_{11/2}h_{11/2}}$ matrix element is this way enhanced from 1.01 to 1.62.

We show in Fig. 8(b) the projection of the symmetric and mixed-symmetric phonon states, but this time, the procedure is repeated with the modified GCN5082 interaction. Of course, a global modification of pairing matrix elements without any further adjustment of the interaction leads to the lowering of the ground state, which is more pronounced than the lowering of the excited 2^+ levels. For example, the 0^+ state in ^{134}Xe is lowered 140 keV more than the 2^+_1 state and 240 keV more than the 2^+_2 state, and thus the whole spectrum gets slightly diluted. Thence, for a better transparency of the comparison in Fig. 8, we have normalized the energies of the first excited 2^+ states in both calculations.

As can now be seen from Fig. 8(b), the symmetric state contribution to the 2^+_1 state remains similar, but the major mixed-symmetric component is shifted to a higher energy. Therefore the agreement of the $B(M1)$ distribution is conspicuously improved, as shown in Fig. 6(b), where $B(M1)$ values calculated with the modified interaction are depicted in comparison to experimental data. In particular, the lowest peak at the energy of about 1.5 MeV is greatly reduced, whereas the $B(M1)$ value of the MSS is slightly enhanced.

Going back to the case of ^{134}Xe, where the improvement is most pronounced, also, the details of the wave function change in a way corresponding to the assumptions made earlier: The first excited 2^+ state is built up by 67% of the $\nu = 2$ neutron component and 21% of the $\nu = 2$ proton component, whereas the MSS changes its character and is now composed of 52% of the $\nu = 2$ proton part and only 24% of the neutron part. The signs of the dominant proton and neutron components in the two states remain opposite. For the completeness of the study, we list the seniority decomposition, proton-neutron couplings, and occupancies of valence shells in these new wave functions in Tables V–VII.

After modifying the pairing matrix elements in the interaction, some changes are brought to the occupation numbers, as well. Although concluding the structure of MSSs from occupancies is not straightforward, two features are noticeable here. First, the original interaction predicts a higher occupancy of the $\pi h_{11/2}$ orbital, which gets reduced when pairing is enhanced globally, in favor of the $\pi d_{5/2}$ orbital. Second, an opposite effect (however, to a lesser extent) is taking place in neutrons, where the $\nu d_{3/2}$ orbital becomes more empty and the $\nu h_{11/2}$ orbital becomes more filled.

TABLE V. Same as Table II, but for GCN5082 interaction with modified pairing elements; see the text for more details.

	J^π	$\nu = 0$	$\nu = 2$ (π, ν)	$\nu = 4$	$\nu = 6$	$\nu > 6$
^{132}Te	0^+	91	0	9	0	0
	2^+_1	0	94 (19,75)	6	0	0
	2^+_2	0	81.5 (41.5,40)	19.5	0	0
^{134}Xe	0^+	82	0	17	1	0
	2^+_1	0	86 (20,66)	10	4	0
	2^+_3	0	73 (49,23)	18	9	0
^{136}Ba	0^+	82	0	17	1	0
	2^+_1	0	86 (21,65)	10	4	0
	2^+_3	0	73 (49,24)	18	9	0
^{138}Ce	0^+	71	0	26	2.5	0.5
	2^+_1	0	75.5 (22.5,53)	14	9.5	1
	2^+_3	0	62 (26,36)	21	14	3
^{140}Nd	0^+	67	0	29	3	1
	2^+_1	0	71.5 (22,49.5)	16.5	11	1
	2^+_3	0	57 (26.5,30.5)	22	18	3

B. Evolution of MS states in $N = 80$ isotones

As mentioned in Sec. I, prior to this work, only the MSSs in $N = 52$ isotones have been studied in the SM approach with an effective interaction derived microscopically [22]. The authors have shown that the evolution of the MSSs in $N = 52$ is mostly driven by the proton orbital part of the magnetic transition operator. It has been also argued that the F-spin symmetry is severely broken near $\pi g_{9/2}$ shell closure, where the collectivity is low, whereas in the middle of the shell, a restoration of the microscopic proton-neutron symmetry is taking place. This is manifested by the parabolic behavior of the $B(M1; 2^+_{\rm MS} \to 2^+_1)$ transitions with a peak in the middle of the shell.

The situation in the $N = 80$ isotones could be a priori different because of the large proton $g_{7/2}$ and $d_{5/2}$ orbitals mixing, imposing no pronounced shell closure in the studied range of Z, as noticed recently in Ref. [19]. No experimental

TABLE VI. Same as Table III, but for a modified interaction.

	J^π	$2^+_\nu \otimes 0^+_\pi$	$0^+_\nu \otimes 2^+_\pi$	$2^+_\nu \otimes 2^+_\pi$
^{132}Te	2^+_1	75	24	4
	2^+_2	40	41	6
^{134}Xe	2^+_1	67	21	5
	2^+_3	24	52	5
^{136}Ba	2^+_1	62	23	6
	2^+_3	34	39	9
^{138}Ce	2^+_1	56	24	7
	2^+_3	38	31	6
^{140}Nd	2^+_1	53	24	9
	2^+_3	34	30	13

TABLE VII. Same as Table IV, but with the modified GCN5082 interaction.

	J^π	$\pi d_{5/2}$	$g_{7/2}$	$s_{1/2}$	$d_{3/2}$	$h_{11/2}$	$\nu d_{5/2}$	$g_{7/2}$	$s_{1/2}$	$d_{3/2}$	$h_{11/2}$
^{132}Te	0^+	0.41	1.38	0.03	0.11	0.07	5.83	7.84	1.81	3.37	11.15
	2^+_1	0.33	1.46	0.03	0.11	0.06	5.86	7.88	1.61	3.31	11.33
	2^+_2	0.29	1.56	0.03	0.08	0.04	5.88	7.91	1.83	3.47	10.90
^{134}Xe	0^+	1.01	2.54	0.07	0.21	0.18	5.80	7.82	1.75	3.26	11.36
	2^+_1	0.95	2.60	0.07	0.21	0.17	5.83	7.85	1.57	3.20	11.55
	2^+_3	0.99	2.56	0.10	0.21	0.14	5.84	7.86	1.78	3.33	11.20
^{136}Ba	0^+	1.73	3.48	0.12	0.32	0.35	5.78	7.80	1.72	3.21	11.48
	2^+_1	1.70	3.50	0.13	0.32	0.35	5.81	7.83	1.56	3.16	11.64
	2^+_3	1.81	3.36	0.19	0.34	0.30	5.85	7.88	1.79	3.30	11.17
^{138}Ce	0^+	2.43	4.33	0.18	0.44	0.62	5.77	7.78	1.70	3.18	11.57
	2^+_1	2.39	4.32	0.20	0.45	0.63	5.79	7.81	1.56	3.13	11.71
	2^+_3	2.54	4.18	0.26	0.48	0.54	5.87	7.91	1.83	3.34	11.04
^{140}Nd	0^+	3.04	5.05	0.26	0.58	1.07	5.76	7.77	1.67	3.15	11.65
	2^+_1	2.94	5.01	0.28	0.61	1.15	5.78	7.79	1.55	3.09	11.79
	2^+_3	3.0	4.91	0.27	0.59	1.22	5.85	7.87	1.75	3.31	11.21

information on magnetic transitions is yet known in the beginning of the shell, that is, in ^{132}Te. The known experimental $B(M1; 2^+_{MS} \rightarrow 2^+_1)$ transitions between ^{134}Xe and ^{138}Ce show a linear decrease, and the fragmentation of the transition grows with proton number, indicating a possible reduction in purity of the mixed-symmetry modes or their disappearance with a further increase of the proton collectivity.

The results of the calculations with both interactions versus experimental data for $B(M1; 2^+_{MS} \rightarrow 2^+_1)$ transitions are depicted in Fig. 9; the contributions of the orbital and spin parts to the $M1$ matrix elements are also displayed. Evidently, the total spin components are negligible compared to the orbital ones, independently of the interaction used. On the contrary, the $B(M1)$ values differ considerably: Though with the genuine interaction [Fig. 9(a)], we predict a decrease of $B(M1)$ from Te to Ce, with its modified version [Fig. 9(b)], a parabolic behavior is found. A measurement in ^{132}Te is necessary to decide in favor of one scenario. Similarly, the original interaction predicts quite a fragmentation of $M1$ strength, whereas its modified version predicts a single peak of $0.2\,\mu_N^2$ around 2.3 MeV in ^{140}Nd. Experiments on ^{140}Nd [35] are of great interest. It is also seen from Fig. 6 that the SM calculations with both interactions fail to reproduce the fragmentation of $M1$ strength onto two closely lying states in ^{138}Ce, as observed in experimentation [17]. This results in a too large total transition value; interestingly, the orbital part of the $B(M1)$ does not vary much from Fig. 9(a) to Fig. 9(b) and fits the experimental value exactly.

Our SM calculations predict that the $M1$ transition between the 2^+_{MS} and the 2^+_1 states is of isovector orbital character. This is in agreement with the expectations of the IBM-2 model. According to this model, the strong $M1$ transition observed between the 2^+_{MS} and the 2^+_1 states in spherical nuclei is similar in nature to the scissor mode observed in deformed nuclei at excitation energies $E \approx 3$ MeV [1,2,36].

Another observable that can shed light on the behavior and formation of the MS states, in addition to the $B(M1)$ values, is the magnetic moment of the calculated state. In the calculations with the GCN5082 interaction [Fig. 10(a)], among excited 2^+ states, the MS state has a magnetic moment closest in value to the magnetic moment of the first 2^+ state, which appears to be because of the similar amplitudes of the proton-neutron content in the wave functions. In Fig. 10(b), we show the behavior of calculated magnetic moments for the first excited and MS 2^+ states using the modified interaction. As can be seen, now the magnetic moments of the 2^+_1 and 2_{MS} states differ one from

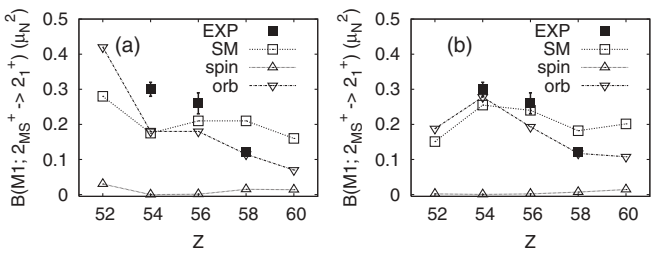

FIG. 9. Evolution of the $B(M1; 2^+_{MS} \rightarrow 2^+_1)$ values in $N = 80$ isotones predicted by SM calculations with the GCN5082 interaction (a) without modifications and (b) with modified pairing matrix elements, compared to available experimental data.

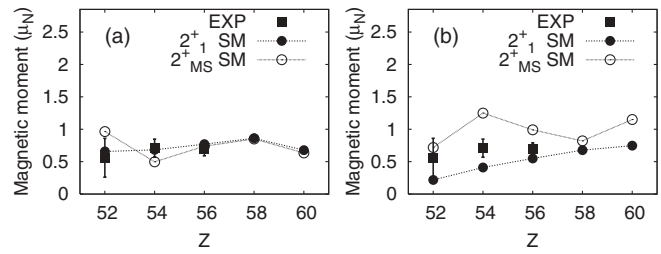

FIG. 10. Magnetic moments of 2^+_1 and 2^+_{MS} states as a function of the proton number, calculated with (a) the genuine GCN5082 interaction and with (b) its modified version. The experimental data concern the first excited 2^+ states.

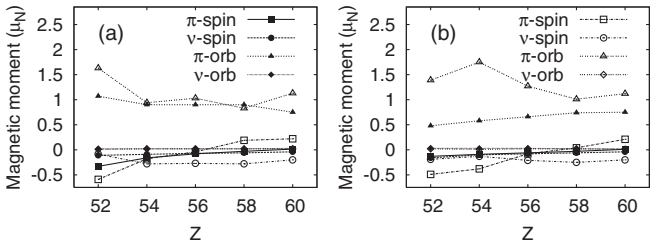

FIG. 11. Calculated proton-neutron and spin-orbital contributions to the magnetic moments. Solid symbols concern the first excited 2^+ state, whereas open symbols concern the mixed-symmetry state: (a) results with the GCN5082 interaction; (b) results with the modified interaction.

another considerably, which reflects the changes brought to the underlying phonon structure.

In Fig. 11, the proton and neutron, spin, and orbital contributions to the moments are plotted. Apparently, the magnetic moments result from a destructive superposition of a large positive orbital part and a smaller negative spin part, both having decreasing tendencies in absolute values when filling proton orbitals. The proton and neutron contributions of a given, i.e., spin-orbital, type are coherent, yet the neutron part is nearly negligible compared to the proton part, which determined the trend of the total magnitude of the magnetic moment as a function of Z.

V. SUMMARY

A fully microscopic study of the MSSs in $N = 80$ isotones has been performed for the first time. Large-scale SM calculations have been carried out for ^{132}Te, ^{134}Xe, ^{136}Ba, ^{138}Ce, and ^{140}Nd in the *gdsh* valence space, using an effective interaction derived for this model space from a realistic nucleon-nucleon Bonn-*C* potential and corrected empirically to reproduce the properties of a large set of nuclei between 50 and 82 shell closures. We have calculated the low-lying excitation spectra of the isotones considered, and a fair agreement with experimental values has been found. The purpose of this work was, however, to study in detail the structure of excited 2^+ states, with a special emphasis on the magnetic transitions between them, which give a hint to the appearance of MSSs. We have shown that realistic calculations reproduce correctly the evolution of the energy spacing between the first excited state and the lowest MSS in known cases, and we have extended the calculations to study neighboring isotones. The effective interaction that has been successful in reproducing a large amount of nuclear data is shown to face difficulty in a more detailed description of the $M1$ transition rates. To understand this deficiency, we have studied in detail the structure of microscopic wave functions, and we have found that the $M1$ transition rates are very sensitive to their seniority structure and hence to the pairing part of the realistic interaction. Thus information on MSSs provides a tool to determine the pairing matrix elements of realistic interactions because they depend very sensitively on the treatment of core polarization corrections [23,37]. Finally, we conclude that the evolution of the $B(M1)$ values of the MSSs in the $N = 80$ isotones is dominated by the isovector orbital part of the $M1$ operator, in analogy to the $N = 52$ isotones studied in Ref. [22]. This observation strengthens the IBM-2 foundations of the MSSs.

ACKNOWLEDGMENTS

We are indebted to E. Caurier and F. Nowacki for letting us use the GCN5082 interaction prior to its publication. We thank also A. Poves and A. Zuker for fruitful discussions. This work has been supported by the state of Hesse within the Helmholtz International Center for FAIR (HIC for FAIR) by the DFG under Grant No. SFB 634.

[1] D. Bohle *et al.*, Phys. Lett. **B137**, 27 (1984).
[2] A. Richter, Prog. Part. Nucl. Phys. **34**, 261 (1995).
[3] N. Pietralla, P. von Brentano, and A. Lisetskiy, Prog. Part. Nucl. Phys. **60**, 225 (2008).
[4] F. Iachello, *Lecture Notes on Theoretical Physics* (Rijksuniversiteit, Groningen, 1976).
[5] T. Otsuka, Ph.D. thesis, University of Tokyo, 1978.
[6] T. Otsuka, A. Arima, F. Iachello, and I. Talmi, Phys. Lett. **B76**, 139 (1978).
[7] F. Iachello and A. Arima, *The Interacting Boson Model* (Cambridge University Press, Cambridge, 1987).
[8] G. Molnar, R. A. Gatenby, and S. W. Yates, Phys. Rev. C **37**, 898 (1988).
[9] P. von Brentano *et al.*, Phys. Rev. Lett. **76**, 2029 (1996).
[10] H. Maser *et al.*, Phys. Rev. C **54**, R2129 (1996).
[11] W. D. Hamilton, A. Irback, and J. P. Elliott, Phys. Rev. Lett. **53**, 2469 (1984).
[12] N. Pietralla *et al.*, Phys. Rev. Lett. **83**, 1303 (1999).
[13] N. Pietralla, C. Fransen, P. vonBrentano, A. Dewald, A. Fitzler, C. Friessner, and J. Gableske, Phys. Rev. Lett. **84**, 3775 (2000).
[14] N. Pietralla *et al.*, Phys. Rev. C **64**, 031301(R) (2001).
[15] T. Ahn *et al.*, Phys. Lett. **B679**, 19 (2009).
[16] K. Lieb *et al.*, Phys. Lett. **B215**, 50 (1998).
[17] G. Rainovski *et al.*, Phys. Rev. Lett. **96**, 122501 (2006).
[18] S. F. Hicks, J. R. Vanhoy, and S. W. Yates, Phys. Rev. C **78**, 054320 (2008).
[19] N. Lo Iudice, C. Stoyanov, and D. Tarpanov, Phys. Rev. C **77**, 044310 (2008).
[20] N. Pietralla *et al.*, Phys. Rev. C **58**, 796 (1998).
[21] A. F. Lisetskiy, N. Pietralla, C. Fransen, R. V. Jolos, and P. von Brentano, Nucl. Phys. **A677**, 100 (2000).
[22] J. D. Holt, N. Pietralla, J. W. Holt, T. T. S. Kuo, and G. Rainovski, Phys. Rev. C **76**, 034325 (2007).
[23] M. Dufour and A. P. Zuker, Phys. Rev. C **54**, 1641 (1996).
[24] E. Caurier, G. Martinez-Pinedo, F. Nowacki, A. Poves, and A. P. Zuker, Rev. Mod. Phys. **77**, 427 (2005).
[25] A. Gniady, E. Caurier, and F. Nowacki (unpublished).
[26] E. Caurier, J. Menendez, F. Nowacki, and A. Poves, Phys. Rev. Lett. **100**, 052503 (2008).

[27] E. Caurier, F. Nowacki, and A. Poves, Eur. Phys. J. **36**, 195 (2008).
[28] J. Menendez, A. Poves, E. Caurier, and F. Nowacki, Nucl. Phys. **A818**, 139 (2009).
[29] A. Shrivastav *et al.* (accepted in Phys. Rev. C).
[30] E. Caurier and F. Nowacki, Acta Phys. Pol. B **30**, 705 (1999).
[31] G. Jakob *et al.*, Phys. Rev. C **65**, 024316 (2002).
[32] N. Pietralla, P. von Brentano, A. Gelberg, T. Otsuka, A. Richter, N. Smirnova, and I. Wiedenhover, Phys. Rev. C **58**, 191 (1998).
[33] T. Otsuka and K.-H. Kim, Phys. Rev. C **50**, R1768 (1994).
[34] A. Poves and G. Martinez-Pinedo, Phys. Lett. **B430**, 203 (1998).
[35] G. Rainovski (unpublished).
[36] N. Pietralla *et al.*, Phys. Rev. C **58**, 184 (1998).
[37] M. Hjorth-Jensen, T. T. S. Kuo, and E. Osnes, Phys. Rep. **261**, 125 (1995).
[38] D. C. Radford *et al.*, Phys. Rev. Lett. **88**, 222501 (2002).
[39] J. McDonald and A. Kerek, Nucl. Phys. **A206**, 417 (1973).
[40] A. Sonzogoni, Nucl. Data Sheets **103**, 1 (2004).
[41] A. Sonzogoni, Nucl. Data Sheets **95**, 837 (2002).
[42] S. Mukhopadhyay *et al.*, Phys. Rev. C **78**, 034317 (2008).
[43] J. J. Valiente-Dobon *et al.*, Phys. Rev. C **69**, 024316 (2004).
[44] A. Sonzogoni, Nucl. Data Sheets **98**, 515 (2003).